Supporting Information

Quantum beat between sunlight and single photons

Zhao-Chen Duan, Yu-Hao Deng, Ying Yu,* Si Chen, Jian Qin, Hui Wang, Xing Ding, Li-Chao Peng, Christian Schneider, Da-Wei Wang,* Sven Höfling, Jonathan P. Dowling, Chao-Yang Lu,* and Jian-Wei Pan

E-mail: yuying26@mail.sysu.edu.cn; dwwang@zju.edu.cn; cylu@ustc.edu.cn

Single-photon source

In our experiment, we use a self-assembled InAs/GaAs quantum dot embedded in a micropillar cavity as the single-photon source. The single-photon resonance fluorescence it generated are experimentally demonstrated to be near-transform-limited with the method described in Reference 1. We study the indistinguishability variation of resonance fluorescence by performing HOM interference of various photon-emission time separations. The indistinguishability decreases from 0.974(1) for 13 ns separation to a plateau of 0.952(3), and the dephasing time is estimated to be on the order of 100 ns with the model derived in Reference 2 (Figure S1a). About this part, please refer Reference 3 and its Supplemental Material for details.

To characterize the Purcell effect of cavity-coupled quantum dot, we measure its emission lifetime of various dot-cavity detuning. The detuning of dot and cavity can be adjusted by changing temperature. At 4 K, the lifetime is measured to be $T_1 = 68.2(3)$ ps, while that of

far-detuning is 431(11) ps (Figure S1b). The Purcell effect is calculated to be 7.4(2) with the standard theoretical formula in Reference 4 (Figure S1c).

We also characterize the spectral profile of single-photon source. The spectrum is acquired using a frequency-tunable continuous-wave laser with a narrow-band of 75 kHz, and that of unfiltered single-photon resonance fluorescence at 4 K shows a Lorentzian profile with the center frequency of ∼335.56 THz (∼893 nm) and full width at half maximum (FWHM) of 2.49(2) GHz. The coherence time can be given from Fourier transform of the spectral profile, yielding $T_2 = 125(1)$ ps (Figure S1d). These results are in good agreement with $T_2 \approx 2T_1$, revealing the high-quality of our single-photon source.

Spectral filtering system

The sunlight has a board continuous spectrum covers from ultraviolet to infrared, while the single-photon resonance fluorescence has a narrow Lorentzian profile with FWHM of ∼2.5 GHz. In order to achieve a good spectra overlap, we firstly implement a series of spectra filters consisting of a tunable band-pass filter, a grating monochromator, and a home-made etalon with a FWHM of ∼5 GHz. The band-pass filter and monochromator are used to coarsely post-select sunlight of wavelength near 893 nm, while the etalon is used for fine tuning by changing the temperature of it. However, the coherence time of single-photon resonance fluorescence without filtering is ∼125 ps, not long enough compared to the time-resolution of detectors. Fortunately, due to the high intensity of our single-photon source, further spectral filtering can be implemented by using narrower etalons.

The etalon is a transparent plate with high reflective surfaces on both sides, leading to Fabry-Pérot interference for impinging light. The optical path length of one round trip is $L = 2nl$, where n is the refractive index of the plate and l is the thickness of it. On the condition that $L = m\lambda$, where $m \in \mathbb{Z}$, the interference will be constructed, showing a series of equidistant peaks in its transparency spectrum. The distance, also called free spectra

range (FSR), is determined by $\Delta_{\mathrm{FSR}} = c/(2nl)$.

The transmission of an etalon with given surface reflectivity R and light frequency ν is

$$T = \frac{1}{1 + F\sin^2(\phi/2)}, \tag{S1}$$

where $F = 4R/(1-R)^2$ and $\phi = 2\pi\nu/\Delta_{\mathrm{FSR}}$. For high surface reflectivity, where $F \to \infty$, Equation (S1) will equivalent to a Lorentzian profile. Figure S2a shows one free spectrum of sunlight after passing the final etalon. The spectra filters are combined in series to eliminate unwanted free spectra.

After both light have been matched, we configure their frequency detuning to be $\Delta =$ 2, 4, 6 and 8 GHz to observe quantum beat. The transmitted frequency (center frequency) of an etalon can be adjusted by changing the thickness of it, which can be done by tuning its temperature. The temperature is controlled and stabled by a proportional-integral-derivative (PID) feedback loop with the fluctuation of ± 5 mK. Figure S2b to S2d show the center frequency changes with temperature for single photons' 1-GHz etalon, sunlight's 1-GHz etalon, and sunlight's 5-GHz etalons. From Figure S2b to S2d, the center frequency is linearly dependent with temperature, with the slope of $-2.57(1)$ GHz/K for single photons' 1-GHz etalon, $-2.41(1)$ GHz/K for sunlight's 1-GHz etalon, and $-2.44(1)$ GHz/K for sunlight's 5-GHz etalon.

Two-photon interference

We define the possibility of n-photon events of sunlight (single photons) to be $P_{S(Q)n}$. In our experiment, the intensities of sunlight and single-photon resonance fluorescence are set to be $\sim$200 kHz and $\sim$150 kHz. Driven by a 76 MHz synchronizing signal, the possibility of more than two-photon events for sunlight are $\sim 1.8 \times 10^{-8}$, which can be neglectable compared to the possibility of $\sim 2.6 \times 10^{-3}$ for single-photon events. Therefore, the initial states of

sunlight and single photons are

$$\begin{aligned}\rho_{\mathrm{Sun}} &= p_{S0}|0\rangle\langle 0| + p_{S1}|1\rangle\langle 1| + p_{S2}|2\rangle\langle 2|,\\ |\phi_{\mathrm{QD}}\rangle &= \sqrt{p_{Q0}}|0\rangle + \sqrt{p_{Q1}}|1\rangle + \sqrt{p_{Q2}}|2\rangle.\end{aligned} \tag{S2}$$

And the joint state is $\rho = \rho_{\mathrm{Sun}} \otimes |\phi_{\mathrm{QD}}\rangle\langle\phi_{\mathrm{QD}}|$.

To analyze two-photon interference, we consider the arriving wave packages of sunlight (single photons) in space-time domain.[5] We denote the creation and annihilation operators for mode k to be $\hat{a}_k^\dagger$ and $\hat{a}_k$ ($k = a$, b, c, or d), and the mode function of sunlight (single photons) to be $\zeta_{\mathrm{Sun(QD)}}(\tau)$.[5] The field operator of detection at detectors c and d can be expressed in

$$\begin{aligned}\boldsymbol{E}_c^+(t) &= \zeta_c(t)\hat{a}_c = \mathrm{i}\sqrt{R}\zeta_{\mathrm{Sun}}(t)\hat{a}_a + \sqrt{T}\zeta_{\mathrm{QD}}(t)\hat{a}_b,\\ \boldsymbol{E}_d^+(t) &= \zeta_d(t)\hat{a}_d = \sqrt{T}\zeta_{\mathrm{Sun}}(t)\hat{a}_a + \mathrm{i}\sqrt{R}\zeta_{\mathrm{QD}}(t)\hat{a}_b,\end{aligned} \tag{S3}$$

where R and T are the reflectivity and transmissivity of the BS. By combining Equations (S2) and (S3), the joint possibility for photon detection events in opposite output ports of BS at time t_0 and $t_0 + \tau$ reads

$$\begin{aligned}P_{\mathrm{joint}}(t_0,\tau) &= \langle \boldsymbol{E}_c^-(t_0)\boldsymbol{E}_d^-(t_0+\tau)\boldsymbol{E}_d^+(t_0+\tau)\boldsymbol{E}_c^+(t_0)\rangle\\ &= 2p_{S2}p_{Q0}RT|\zeta_{\mathrm{Sun}}(t_0)\zeta_{\mathrm{Sun}}(t_0+\tau)|^2\\ &+ p_{S1}p_{Q1}|R\zeta_{\mathrm{Sun}}(t_0)\zeta_{\mathrm{QD}}(t_0+\tau) - T\zeta_{\mathrm{Sun}}(t_0+\tau)\zeta_{\mathrm{QD}}(t_0)|^2\\ &+ 2p_{S0}p_{Q2}RT|\zeta_{\mathrm{QD}}(t_0)\zeta_{\mathrm{QD}}(t_0+\tau)|^2.\end{aligned} \tag{S4}$$

And the second order correlation function can be computed by Equation (S4) via

$$\mathcal{G}^{(2)}(\tau) = \int \mathrm{d}t_0 P_{\mathrm{joint}}(t_0,\tau) = \mathcal{G}^{(2)}_{\mathrm{Sun}}(\tau) + \mathcal{G}^{(2)}_{\mathrm{int}}(\tau) + \mathcal{G}^{(2)}_{\mathrm{QD}}(\tau), \tag{S5}$$

where the first and third terms on the right hand of Equation (S5) are contributed from the second order coherence of sunlight and single photons, which can be determined experimen-

tally.[5] After having been subtracted from these terms, the cross-correlation term of Equation (S5), which corresponds to two-photon interference only, leads to

$$\mathcal{G}^{(2)}_{\mathrm{int}}(\tau) = p_{S1}p_{Q1}\int \mathrm{d}t_0 |R\zeta_{\mathrm{Sun}}(t_0)\zeta_{\mathrm{QD}}(t_0+\tau) - T\zeta_{\mathrm{Sun}}(t_0+\tau)\zeta_{\mathrm{QD}}(t_0)|^2. \tag{S6}$$

One of the most dramatic feature of Equation (S6) is that at zero-delay it only depends on the balance of the BS. Equation (S6) can be further transformed to

$$\begin{aligned}\mathcal{G}^{(2)}_{\mathrm{int}}(\tau) = p_{S1}p_{Q1}\Big[R^2\int \mathrm{d}t_0|\zeta_{\mathrm{Sun}}(t_0)\zeta_{\mathrm{QD}}(t_0+\tau)|^2 + T^2\int \mathrm{d}t_0|\zeta_{\mathrm{Sun}}(t_0+\tau)\zeta_{\mathrm{QD}}(t_0)|^2 \\ + \int \mathrm{d}t_0|\zeta_{\mathrm{Sun}}(t_0)\zeta_{\mathrm{Sun}}(t_0+\tau)\zeta_{\mathrm{QD}}(t_0)\zeta_{\mathrm{QD}}(t_0+\tau)|\Big].\end{aligned} \tag{S7}$$

The former two terms of Equation (S7) correspond to the behavior of distinguishable photons, and indistinguishable photons will influence the last term that let Equation (S7) to vanish at zero-delay. Here, we use $\mathcal{G}^{(2)}_{\parallel(\perp)}(\tau)$ to represent indistinguishable (distinguishable) terms. As the sunlight and single photons after passing etalon have the Lorentzian profile in spectra, the mode functions of them will show in the form

$$\zeta(t) = \begin{cases}\sqrt{2\sigma}\,\mathrm{e}^{-\sigma t - \mathrm{i}\omega t} & ,t \geq 0 \\ 0 & ,t<0\end{cases}. \tag{S8}$$

We introduce the parameter V as the visibility of our HOM interference. By combining Equations (S7) and (S8), the second-order cross-correlation function will be

$$\mathcal{G}^{(2)}_{\parallel}(\tau) = \mathcal{G}^{(2)}_{\perp}(\tau) - 2p_{S1}p_{Q1}RTV\,\mathrm{e}^{-\sigma|\tau|}\cos(\Delta\tau) \tag{S9}$$

For a balanced BS, the reflectivity and transmissivity satisfy $R = T = 1/2$. As the visibility can be estimated by $V = 1 - \mathcal{G}^{(2)}_{\parallel}(0)/\mathcal{G}^{(2)}_{\perp}(0)$, Equation (S9) will lead to

$$\mathcal{G}^{(2)}_{\parallel}(\tau) = \mathcal{G}^{(2)}_{\perp}(\tau)[1 - V\,\mathrm{e}^{-\sigma|\tau|}\cos(\Delta\tau)]. \tag{S10}$$

Optimal intensity ratio

As the sunlight is temporally continuous and bunching, temporally irrelevant multi-photon events from sunlight can be discarded. In our experiment, we implement an electrical window that gates our detectors ON only when single photon pulse comes. From Equation (S6), the ideal two-photon interference can achieve 100 % visibility. As the QD is not a perfect single-photon source, the multi-photon contribution from it must be taken into consideration. In this condition, too strong and too weak sunlight or single photons both result in a non-vanishing HOM dip. Therefore, the intensity ratio between dissimilar light fields need to be determined to achieve a better raw visibility.

We denote the pulse period and gate width as T_P and T_G. By introducing the electrical gate, the contribution from sunlight can be suppressed by a factor of T_P/T_G. The coincidence events to be registered must satisfy the condition that

$$\mathbb{G} = \left\{(t_0, \tau)\middle||t_0| \leq \frac{T_G}{2}, |t_0 + \tau| \leq \frac{T_G}{2}\right\}. \tag{S11}$$

Under low efficiency regime of our experiment, the possibilities of n-photon events satisfy $p_0 \approx 1$ and $g^{(2)}(0) = 2p_2/p_2^2$. Here, we define $I_{\mathrm{Sun(QD)}} = p_{S(Q)1}$ to be intensities of sunlight (single photons). As the sunlight is continuous in time, while single photons are pulsed, each

term of Equation (S5) reads

$$\begin{aligned}
\mathcal{G}^{(2)}_{\mathrm{Sun}}(\tau) &= \frac{2}{T_P^2} p_{S2} p_{Q0} RT \int_{\mathbb{G}} \mathrm{d}t_0 |\zeta_{\mathrm{Sun}}(t_0)\zeta_{\mathrm{Sun}}(t_0+\tau)|^2 \\
&= \frac{T_G I^2_{\mathrm{Sun}}}{4T_P^2} g^{(2)}_{\mathrm{Sun}}(\tau), \\
\mathcal{G}^{(2)}_{\mathrm{int}}(\tau) &= \frac{1}{T_P} p_{S1} p_{Q1} \int_{\mathbb{G}} \mathrm{d}t_0 |R\zeta_{\mathrm{Sun}}(t_0)\zeta_{\mathrm{QD}}(t_0+\tau) - T\zeta_{\mathrm{Sun}}(t_0+\tau)\zeta_{\mathrm{QD}}(t_0)|^2 \\
&= \frac{I_{\mathrm{Sun}} I_{\mathrm{QD}}}{2T_P} g^{(2)}_{\mathrm{int}}(\tau), \\
\mathcal{G}^{(2)}_{\mathrm{QD}}(\tau) &= 2 p_{S0} p_{Q2} RT \int_{\mathbb{G}} \mathrm{d}t_0 |\zeta_{\mathrm{QD}}(t_0)\zeta_{\mathrm{QD}}(t_0+\tau)|^2 \\
&= \frac{\sigma_{\mathrm{QD}} I^2_{\mathrm{QD}}}{4} g^{(2)}_{\mathrm{QD}}(\tau).
\end{aligned} \tag{S12}$$

We denote $V_{\mathrm{raw(corr)}}$ to be raw (corrected) HOM visibility, the relation between them will be

$$\begin{aligned}
V_{\mathrm{raw}} &= \frac{\mathcal{G}^{(2)}_{\perp}(0) - \mathcal{G}^{(2)}_{\parallel}(0)}{\mathcal{G}^{(2)}_{\mathrm{Sun}}(0) + \mathcal{G}^{(2)}_{\perp}(0) + \mathcal{G}^{(2)}_{\mathrm{QD}}(0)} \\
&= \frac{\frac{I_{\mathrm{Sun}} I_{\mathrm{QD}}}{2T_P} g^{(2)}_{\mathrm{int}}(0) V_{\mathrm{corr}}}{\frac{T_G I^2_{\mathrm{Sun}}}{4T_P^2} g^{(2)}_{\mathrm{Sun}}(0) + \frac{I_{\mathrm{Sun}} I_{\mathrm{QD}}}{2T_P} g^{(2)}_{\mathrm{int}}(0) + \frac{\sigma_{\mathrm{QD}} I^2_{\mathrm{QD}}}{4} g^{(2)}_{\mathrm{QD}}(0)}.
\end{aligned} \tag{S13}$$

Equation (S13) can be further transformed to

$$\frac{V_{\mathrm{corr}}}{V_{\mathrm{raw}}} = 1 + \frac{T_G}{2T_P} \frac{I_{\mathrm{Sun}}}{I_{\mathrm{QD}}} g^{(2)}_{\mathrm{Sun}}(0) + \frac{T_P \sigma_{\mathrm{QD}}}{2} \frac{I_{\mathrm{QD}}}{I_{\mathrm{Sun}}} g^{(2)}_{\mathrm{QD}}(0). \tag{S14}$$

By solving Equation (S14), the optimal sunlight-single photon intensity ratio gives

$$\frac{I^2_{\mathrm{Sun}} g^{(2)}_{\mathrm{Sun}}(0)}{I^2_{\mathrm{QD}} g^{(2)}_{\mathrm{QD}}(0)} = \frac{T_P^2 \sigma_{\mathrm{QD}}}{T_G}. \tag{S15}$$

Interstella extension

In current experimental configuration with the Sun, the experimental data are accumulated within 40 min. The Supplemental Material of Reference 3 analyses the interference between quantum dot and Sirius (an extrasolar object), the data accumulation time can be shorten with purer single-photon source.

References

(1) Wang, H.; Duan, Z.-C.; Li, Y.-H.; Chen, S.; Li, J.-P.; He, Y.-M.; Chen, M.-C.; He, Y.; Ding, X.; Peng, C.-Z., et al. *Phys. Rev. Lett.* **2016**, *116*, 213601.

(2) Thoma, A.; Schnauber, P.; Gschrey, M.; Seifried, M.; Wolters, J.; Schulze, J.-H.; Strittmatter, A.; Rodt, S.; Carmele, A.; Knorr, A., et al. *Phys. Rev. Lett.* **2016**, *116*, 033601.

(3) Deng, Y.-H.; Wang, H.; Ding, X.; Duan, Z.-C.; Qin, J.; Chen, M.-C.; He, Y.; He, Y.-M.; Li, J.-P.; Li, Y.-H., et al. *Phys. Rev. Lett.* **2019**, *123*, 080401.

(4) Fox, M. *Quantum Optics: An Introduction*; Oxford University Press: Oxford, **2006**.

(5) Legero, T.; Wilk, T.; Kuhn, A.; Rempe, G. *Appl. Phys. B: Lasers Opt.* **2003**, *77*, 797–802.

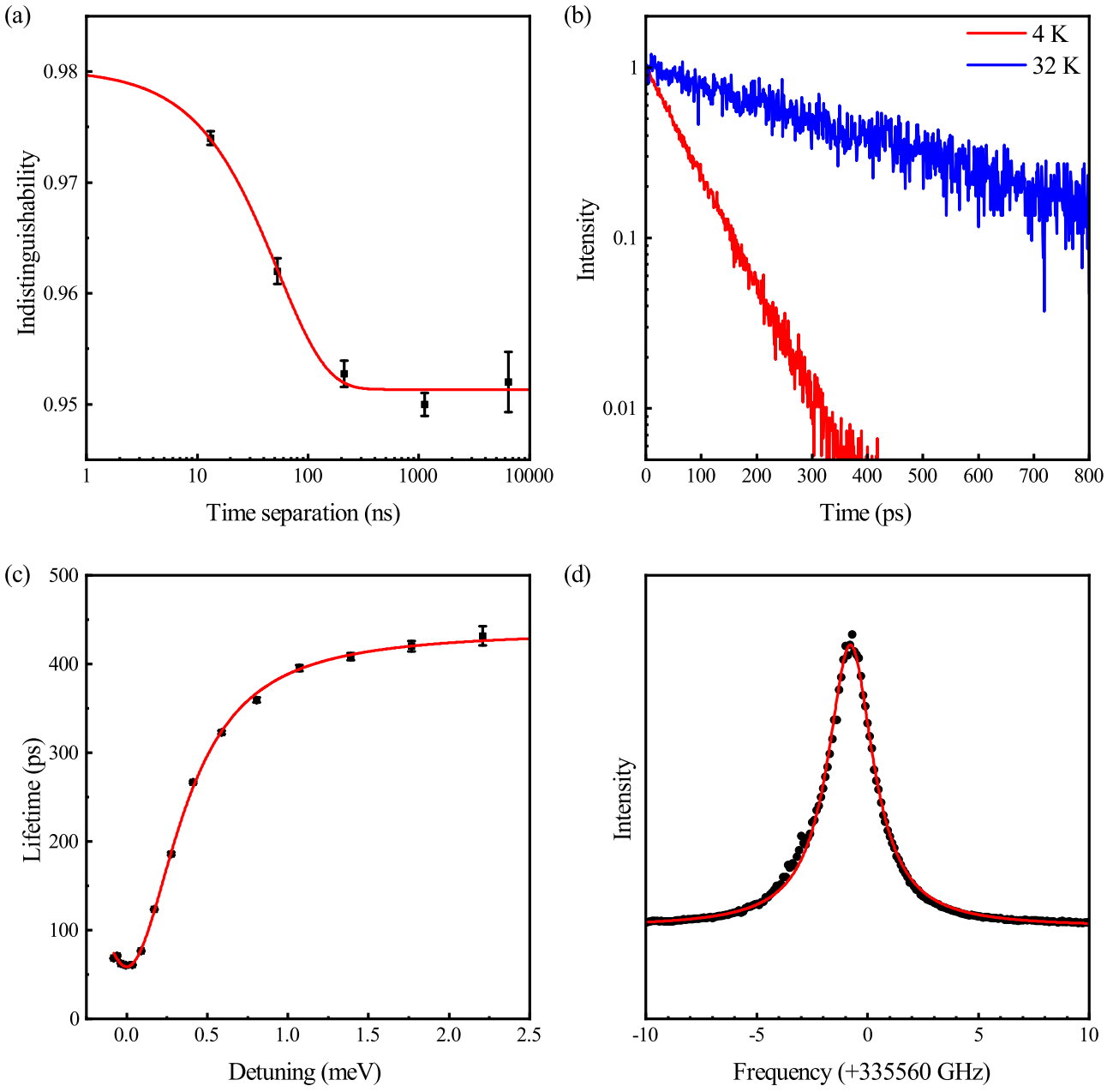

Figure S1: (a) The corrected indistinguishability of various photon-emission time separations. The x-axis is in logarithmic scale to highlight data both in short- and long-timescale. The red curve is fitted with the method derived in Reference 2, and the dephasing time is estimated to be on the order of 100 ns. This plot is taken from Supplemental Material of Reference 3 (b) Examples of time-resolved counts of dot-cavity system at 4 K (near-resonance) and 32 K (far-detuning). (c) The lifetime of different dot-cavity detuning. Dot-cavity detuning is determined by changing temperature. The red curve is fitted with the standard theoretical formula in Reference 4, revealing the Purcell factor of 7.4(2). (d) Spectra profile of unfiltered single photons. The spectrum shows a Lorentzian profile with the center frequency (wavelength) of ∼335.56 THz, and a FWHM of 2.49(2) GHz. The Fourier transform of it gives the coherence time of 125(1) ps.

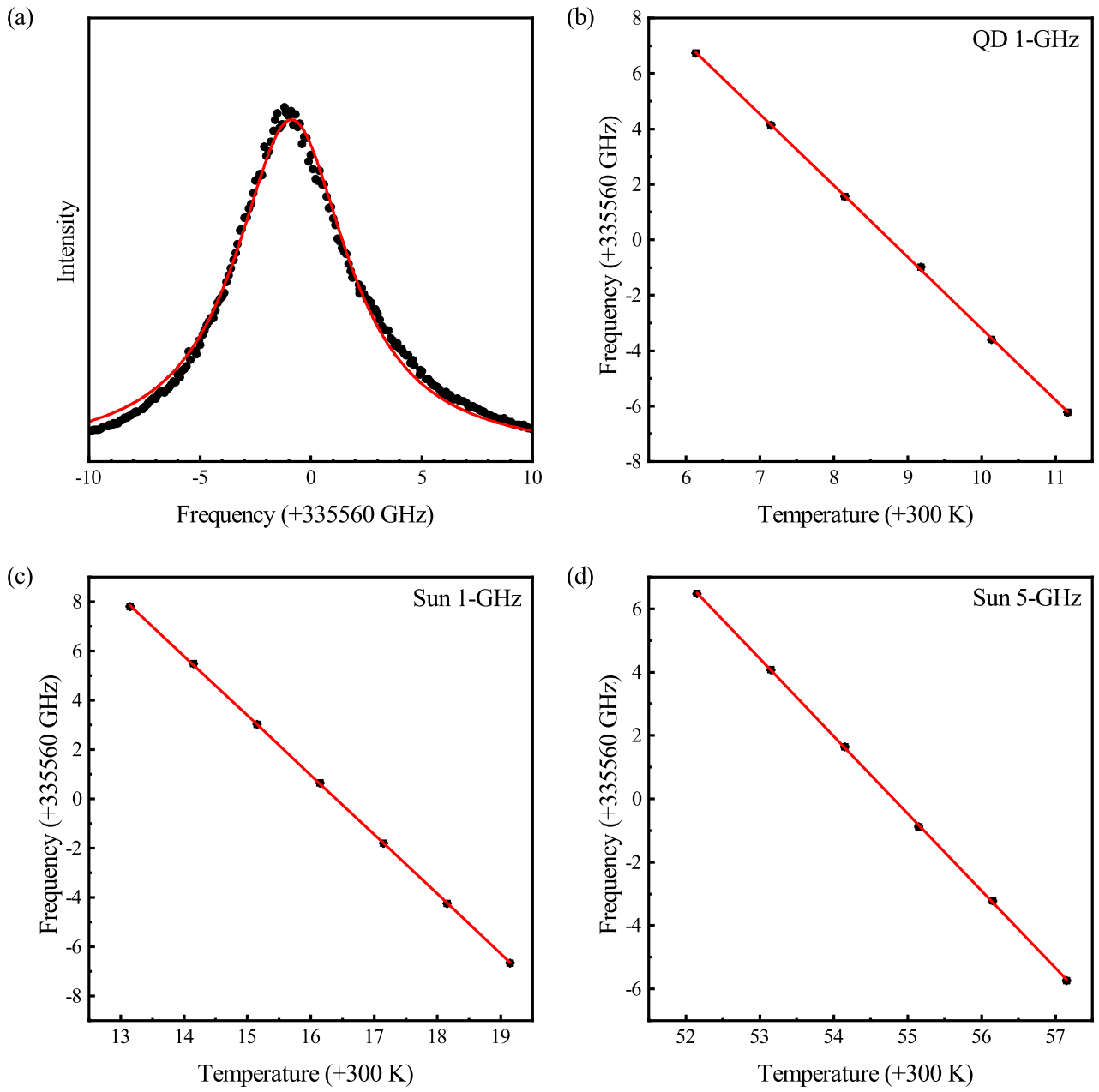

Figure S2: (a) Spectra profile of sunlight after passing 5-GHz etalon. The spectrum is similar as that shown in Figure S1d with a FWHM of ∼5 GHz. (b–d) Center frequency verses temperature for (b) single photons' 1-GHz etalon, (c) sunlight's 1-GHz etalon, and (d) sunlight's 5-GHz etalon. Within the temperature region under study the center frequency is well described to be of linear dependence on temperature with slopes of (b) −2.57(1) GHz/K for single photons' 1-GHz etalon, (c) −2.41(1) GHz/K for sunlight's 1-GHz etalon, and (d) −2.44(1) GHz/K for sunlight's 5-GHz etalon.